Molecular Cell
Short Article

An Unusual Allosteric Mobility of the C-Terminal Helix of a High-Affinity α_L Integrin I Domain Variant Bound to ICAM-5

Hongmin Zhang,[1,2] Jose M. Casasnovas,[5] Moonsoo Jin,[6] Jin-huan Liu,[1,2] Carl G. Gahmberg,[7] Timothy A. Springer,[6] and Jia-huai Wang[1,3,4,*]
[1]Department of Medical Oncology and Department of Cancer Biology, Dana-Farber Cancer Institute, 44 Binney Street, Boston, MA 02115, USA
[2]Department of Medicine
[3]Department of Pediatrics
[4]Department of Biological Chemistry and Molecular Pharmacology
Harvard Medical School, Boston, MA 02115, USA
[5]Centro Nacional de Biotecnología, CSIC, Campus Universidad Autónoma, 28049 Madrid, Spain
[6]Immune Disease Institute and Department of Pathology, Harvard Medical School, 200 Longwood Avenue, Boston, MA 02115, USA
[7]Division of Biochemistry, University of Helsinki, Viikinkaari 5, 00014 Helsinki, Finland
*Correspondence: jwang@red.dfci.harvard.edu
DOI 10.1016/j.molcel.2008.06.022

SUMMARY

Integrins are cell surface receptors that transduce signals bidirectionally across the plasma membrane. The key event of integrin signaling is the allosteric regulation between its ligand-binding site and the C-terminal helix (α7) of integrin's inserted (I) domain. A significant axial movement of the α7 helix is associated with the open, active conformation of integrins. We describe the crystal structure of an engineered high-affinity I domain from the integrin $\alpha_L\beta_2$ (LFA-1) α subunit in complex with the N-terminal two domains of ICAM-5, an adhesion molecule expressed in telencephalic neurons. The finding that the α7 helix swings out and inserts into a neighboring I domain in an upside-down orientation in the crystals implies an intrinsically unusual mobility of this helix. This remarkable feature allows the α7 helix to trigger integrin's large-scale conformational changes with little energy penalty. It serves as a mechanistic example of how a weakly bound adhesion molecule works in signaling.

INTRODUCTION

Integrins are among the most important cell adhesion molecules in metazoa. They play a key role in development, immune responses, leukocyte trafficking, homeostasis, and cancer. Composed of noncovalently linked α and β transmembrane subunits, integrin molecules transduce signals across the plasma membrane bidirectionally in an allosteric fashion. Ligand binding to these receptors transduces signals to the cytoplasm, called "outside-in" signaling. On the other hand, integrins can be activated by other receptors to have higher affinity to ligand through its cytoplasmic portion, a process named "inside-out" signaling (Hynes, 2002; Springer and Wang, 2004). The structural basis of integrin allostery has recently been extensively reviewed (Luo et al., 2007). In about half of the integrins, ligand primarily binds to the I domain, which is inserted within the β propeller domain. The β subunits contain an I-like domain, which is inserted within the hybrid domain. The ligand-binding site of I domains has a bound metal ion coordinated by residues in loops that constitute the metal ion-dependent adhesion site (MIDAS). Upon ligand-binding, an acidic residue from the ligand completes the coordination of the metal ion, changing the conformation of MIDAS loops, which is allosterically linked to an axial movement of the α7 helix at the other end of the I domain. This eventually triggers a large-scale reorientation of integrin's ectodomains up to 200 Å, and the separation of the integrin α and β subunits by as much as 70 Å. Conversely, an inside signal can cause alterations in MIDAS, which facilitate ligand binding (Luo et al., 2007). The allosteric movement of the α7 helix was first discovered in the crystal structure of the I domain from the integrin $\alpha_M\beta_2$ (Lee et al., 1995). The observation has been confirmed by cocrystal structures of I domains with physiological ligands, including the I domain of integrin $\alpha_2\beta_1$ in complex with a triple helical collagen peptide (Emsley et al., 2000), and the I domain of integrin $\alpha_L\beta_2$ in complex with ICAM-1 (Shimaoka et al., 2003) and ICAM-3 (Song et al., 2005).

ICAM-1 and ICAM-3 both belong to the intercellular adhesion molecule (ICAM) family, forming a subfamily of the large immunoglobulin superfamily (IgSF). The five described ICAM members (ICAM-1, -2, -3, -4, and -5) share much more sequence identity with one another (30%–50%) than with other IgSF members. All ICAM family members bind to the I domain of integrin $\alpha_L\beta_2$ (Gahmberg, 1997). Within the family, ICAM-5 (telencephalin) is unique in a number of regards. It is composed of nine Ig-like domains as opposed to two or five Ig-like domains for other family members. The ICAMs have distinct tissue distributions. ICAM-1, -2, and -3 are expressed on leukocyte surfaces. In addition, ICAM-1 and -2 are also expressed on endothelium. These three molecules perform immune function through binding to

leukocyte integrins. By contrast, ICAM-5's expression is restricted to the neurons of the gray matter of the telencephalon, a region in the central nervous system (CNS) that takes charge of higher brain functions such as memory, learning, emotion, etc. (Mori et al., 1987; Oka et al., 1990). In CNS, $\alpha_L\beta_2$ is constitutively expressed by microglia, the brain-type macrophage. The findings that ICAM-5 acts as a cellular ligand for integrin $\alpha_L\beta_2$ (Mizuno et al., 1997; Tian et al., 1997), and the fact that binding induces rapid spreading of microglia and clustering of $\alpha_L\beta_2$ on the surface of spreading microglia (Mizuno et al., 1999) provide a basis for understanding the underlying cell-cell interactions between ICAM-5-expressing telencephalic neurons and $\alpha_L\beta_2$-expressing microglia in pathological as well as physiological contexts. More recently, a soluble ICAM-5 molecule has been found to be cleaved from neurons, which may regulate the immune response in the CNS (Lindsberg et al., 2002), acting as an anti-inflammatory agent (Tian et al., 2008).

Here we report the crystal structure of an engineered high-affinity I domain of integrin $\alpha_L\beta_2$ in complex with the ICAM-5 N-terminal two domains. The high-affinity I domain incorporates two mutations selected by directed evolution, an approach based on random mutagenesis coupled with functional screening. The double mutation of F265S/F292G confers 200,000-fold ICAM-1 binding affinity increase to the I domain compared to the wild-type I domain (Jin et al., 2006), which facilitates the cocrystallization of the I domain with the otherwise weakly bound ICAM-5. The structure confirms the conclusion we drew earlier (Song et al., 2005) that all ICAM family members share an identical docking mechanism onto the α_L I domain. The most interesting feature of the current structure is that the α7 helix swings out of the I domain and docks onto the neighboring I domain in an upside-down orientation in the crystal space. It demonstrates the extremely loose packing of this helix against the major body of the domain and shows that there is virtually no rigorous requirement for the side-chain interaction specificity between this helix and the rest of molecule, nor even for the helical polarity. The unusual intrinsic mobility of this helix is the prerequisite of this kind of allostery for integrin signaling. The structure also explains why ICAM-5 has a low affinity compared to other ICAM family members and how the double mutant α_L I domain (dm-I domain) results in high affinity.

RESULTS

Structure of the ICAM-5/dm-I Domain

The ICAM-5 N-terminal two-domain fragment was expressed in Lec3.2.8.1 Chinese hamster ovary (CHO) cells. Since all ICAM family members have low binding affinity to wild-type α_L I domain, the protein was subjected to cocrystallization with engineered α_L I domains of higher affinity than the wild-type. An engineered disulfide bond introduced into the I domain stabilizes the domain in intermediate (IA) and open conformations (HA) with affinity 500- and 10,000-fold higher than wild-type, respectively (Shimaoka et al., 2003). The IA and HA mutants have been successfully used in cocrystallization with ICAM-1 (Shimaoka et al., 2003) and ICAM-3 (Song et al., 2005), respectively. However, neither the IA nor HA mutant worked for ICAM-5 cocrystallization. We then turned to the recently identified dm-I domain, the double mutant (F265S/F292G) I domain that has 20-fold higher affinity to ICAM-1 than the HA mutant (Jin et al., 2006). Nice orthorhombic cocrystals grew. The ICAM-5/dm-I domain complex structure was determined using molecular replacement as described in the Experimental Procedures. The data statistics of structure determination and refinement are listed in Table 1. Figure 1 is a ribbon diagram of the complex structure. Also shown in Figure S1 (available online) are eight such complexes along crystal screw axis 2_1, which gives a better view about how these molecules pack in crystal.

Table 1. Data Collection and Refinement Statistics

Space group	$P2_12_12_1$
a (Å)	61.8
b (Å)	71.5
c (Å)	143.9
Molecule/asymmetric unit	1
Wavelength (Å)	0.97931
Resolution (Å)	50–2.1
Unique reflections	37303
Completeness (%)	98.6 (95.5)
R_{sym}[a] (%)	7.2 (45.4)
$I/\sigma(I)$	26.5 (3.8)
Redundancy	8.2 (5.6)
Ref reflections (work/test)	35440/1863
R^b/R_{free} (%)	19.08/23.49
Ramachandran plot (favored/allowed/outlier %)	98.1/1.9/0
Protein residues/Mg^{2+}/NAG/glycerol/waters	376/1/6/2/226
Average B factor (Å^2)	43.7
Rmsd from ideal values	
Bond lengths (Å)	0.009
Bond angles (°)	1.320

Numbers in parentheses are for the highest-resolution shell.
[a] $Rsym = \sum_{hkl}|I - < I >|/\sum I$, where I is the observed intensity and $< I >$ is the average intensity from observations of symmetry-related reflections. A subset of the data (5%) was excluded from the refinement and used to calculate R_{free}.
[b] $R = \sum||Fo| - |Fc||/\sum|Fo|$.

The I domain binds to the N-terminal domain (D1) of ICAM-5. The docking mode of ICAM-5 D1 to I domain is identical to that of ICAM-1 and ICAM-3. Figure 2A is an overlay of the ICAM-3 complex structure onto the ICAM-5 complex. The superposition based on the I domains brings the two ICAM D1 domains into alignment. Interestingly, the key I domain-binding residue Glu37 from two ICAM molecules assumes the same conformation. The dm-I domain is indeed in the open conformation as expected. Despite the absence of a disulfide bond to lock the I domain into the HA form, the conformation of the dm-I domain in the ICAM-5 complex can be superposed onto that of HA in the ICAM-3 complex extremely well up to the residue Ile288 with the RMSD value of 0.67 Å (Figure 2A), as opposed to 1.40 Å for the corresponding IA in the ICAM-1 complex (Protein Data Bank [PDB] code 1MQ8) superposition. This includes all residues

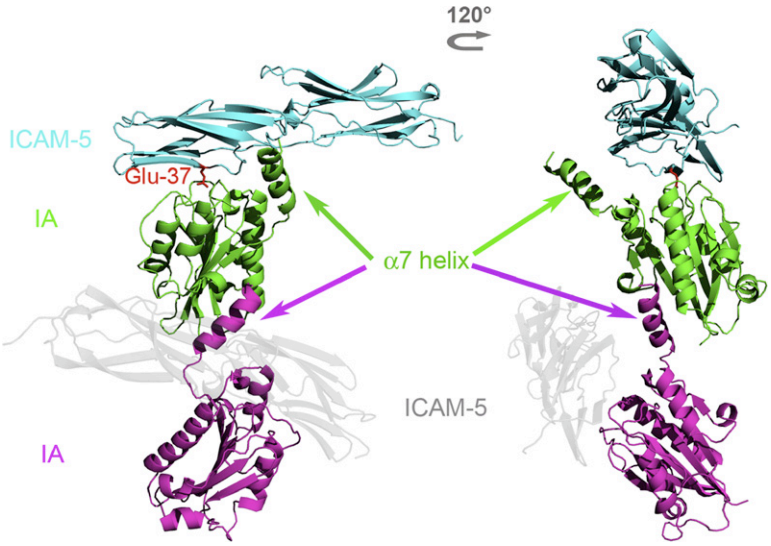

Figure 1. Ribbon Diagram of the ICAM-5/dm-I Complex

Two symmetry-related complexes of the ICAM-5/dm-I domain are shown. In one complex ICAM-5 is in cyan and the I domain in green. In the other complex the I domain is in magenta and the ICAM-5 molecule is in shadow for clarity. The C-terminal α7 helix of the magenta I domain inserts into a groove in the green I domain in an upside-down fashion. Glu-37 in ICAM-5 D1 that binds to the I domain's MIDAS is shown in red as a ball-and-stick model. The figures are all prepared with Pymol (http://www.pymol.org/).

involved in the ligand-binding "active site," the MIDAS. Figure 2C is a local illustration of the involving area for three superposed structures: the dm-I domain in ICAM-5 complex (in green), the HA in the ICAM-3 complex (PDB code 1T0P, in cyan), and the closed form of the α_L I domain (PDB code 1ZOP, in magenta). Binding of the Glu37 of a ligand to both the HA and dm-I domains triggers a 2 Å movement of the metal ion from that seen in the closed conformation of the I domain. Consequently, the direct coordination of MIDAS residue Asp239 is replaced by an indirect coordination through a water molecule (Figure 2C). This triggers a series of conformational changes that are typical to the open form, but absent in the closed form assumed by the wild-type α_L I domain. However, quite unexpectedly, in the ICAM-5 complex the region between Leu289 and the end of the α7 helix in the dm-I domain dramatically changes its orientation. The segment of Asp290–Glu293 no longer bends into the β6α7 loop as seen in the wild-type structure. Instead, this segment now assumes an extended conformation. As a result, the entire α7 helix swings 180° out of the domain (Figure 2A). Intriguingly, the α7 helix fits into a symmetry-related dm-I domain molecule in a very similar location to that seen in the ICAM-3 complex structure, but running in the opposite direction (Figures 1 and 2A). In Figure 1, the I domain shown in magenta color from the symmetry-related complex has its α7 helix fitting

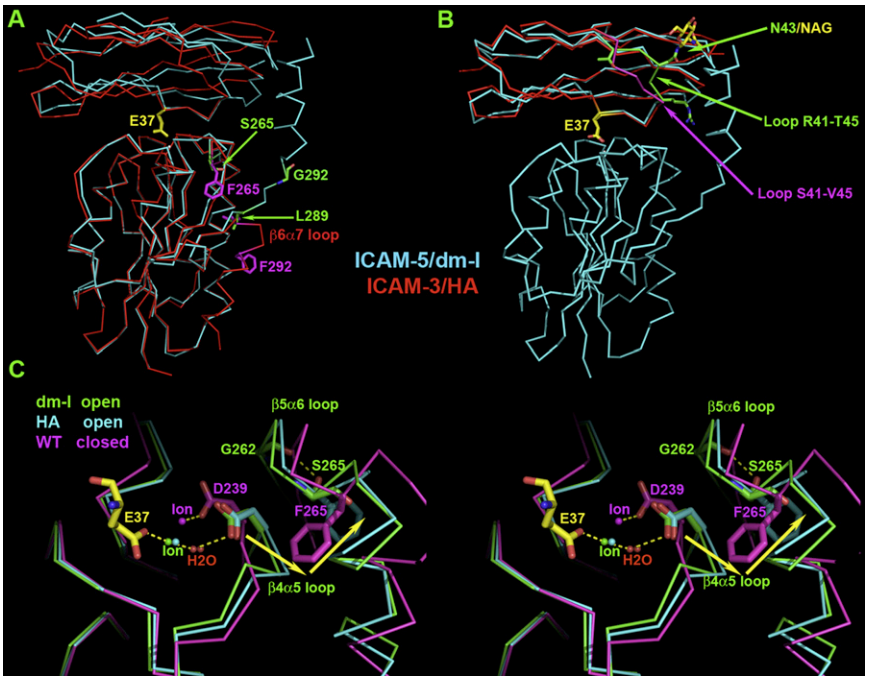

Figure 2. Superimposition of the ICAM-3/HA Complex onto the ICAM-5/dm-I Complex

ICAM-3/HA is in red and the ICAM-5/dm-I complex is in cyan. For clarity, the ICAM-5 D2 is not shown in the figures. The conserved Glu-37 is in yellow.

(A) The superposition is based on I domains. Side chains at the two mutation sites are shown in a ball-and-stick model with Phe265 and Phe292 in the HA replaced by Ser265 and Gly292 in the dm-I domain, respectively. Also shown are Leu289s where the polypeptide chains of the two I domains start to run opposite directions.

(B) The ICAMs' domain D1s were used for superposition. HA I domain from the ICAM-3/HA complex is not shown for clarity. The loops of R41-T45 in ICAM-5 and S41-V45 in ICAM-3 are colored green and magenta, respectively. Residue N43 and attached sugar NAG-2 from ICAM-5 D1 are also shown as a ball-and-stick model.

(C) The stereo view of the local region around MIDAS of superimposed I domains. The I domain from ICAM-5 complex is in green, that from the ICAM-3 complex is in cyan, and the closed form of the α_L I domain (1ZOP) in magenta. Glu-37 from ICAM-5 that binds to MIDAS is shown in yellow. The metal ion is shown as a ball. Side chains of residues D239, S265, F265, and G262 are labeled and shown in a ball-and-stick model. The yellow arrows indicate the movement direction of the β4α5 loop and the F265 ring from closed form to open form.

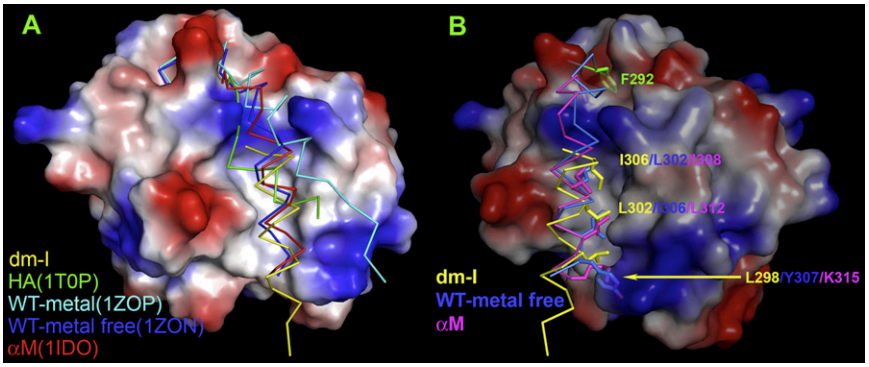

Figure 3. Diverse Orientation of α7 Helix

I domains from different structures are superimposed.

(A) Front view of a surface representation of the I domain from ICAM-5 complex with α7 helices from other structures overlaid. Note that the five α7 helices assume their distinct orientations within the conic groove.

(B) Side view of (A). Only α7 helices from the I domain in the ICAM-5 complex, the α_L I domain in metal-free form, and the α_M I domain are shown for clarity. Hydrophobic residues forming hydrophobic interactions with the groove are shown with side chains. They are Leu302, Ile306, and Tyr307 in the metal-free α_L I domain as well as Ile308, Leu312, and the aliphatic portion of Lys315 in the α_M I domain from the top down. For the dm-I domain, they are Ile306, Leu302, and Leu298 in a reverse order. Also noticeable is the relatively hydrophobic pocket at the top of the figure, which accommodates the phenol ring of Phe292 (in green shade) in its closed form.

into the I domain in green color of the complex. The electron densities unambiguously define the tracing and the helical polarity of the segment of Asp290–Glu293 (maps are not shown).

As in other ICAM complex structures studied, the major contributions to the interaction in ICAM-5 D1 are the CD loop and the C and F strands on the Ig-like domain's GFC β sheet. The conserved Glu37 sits at the center of the interface as the hot spot to complete metal coordination on MIDAS (Figure 2B). The distinct feature of ICAM-5 is that the conformations of the end of the CD loop and the beginning of the D strand (from Arg41 to Thr45) are very different from that of other ICAM family members (Figure 2B). These differences could be related to the presence of a unique glycosylation site attached to the Asn43 residue at the CD loop of ICAM-5, absent in the other ICAM proteins.

The Diverse Positioning of α7 Helix and the "Conical Groove"

To better study the unusual positioning of the α7 helix in the ICAM-5 complex, we have collected five representative conformations of the α7 helix of the I domain from different structures and overlaid them on the dm-I domain from the ICAM-5 complex (Figure 3A). In this figure, the surface representation was generated from the dm-I domain. A conical groove that opens toward the bottom of the domain can be clearly seen. Lying in this groove in the Figure 3A are four peptide segments of the α_L I domain beginning from Leu289 to the end of the α7 helix, taken from the structures of the ICAM-5 complex (in yellow), the ICAM-3 complex (in green), and the unligated I domain in Mn^{2+} ion-chelating form (in cyan, PDB code 1ZOP) and in metal-free form (in blue, PDB code 1ZON). The first two are from the open conformation, whereas the last two are from the closed conformation. In addition, a corresponding α7 helix from the α_M I domain beginning at Phe297 (in red, PDB code 1IDO) is also included. In that structure, a glutamic acid residue from the neighboring molecule in crystal space mimics ligand binding, causing the αM I domain to assume an open conformation (Lee et al., 1995). This compilation of α7 helices in the Figure 3A is striking in the diversity of their positioning within the conical groove. The five helices fall into two categories. The α7 helix from the ICAM-5 complex and that of metal-free α_L I domain and α_M I domain all deeply fit into the central entrenchment-like structure within the groove. By contrast, the α7 helix of the HA in the ICAM-3 complex and that of the Mn^{2+} ion-chelating form of the α_L I domain are dislocated by an engineered disulfide bond for the former (Song et al., 2005) and the crystal packing for the latter (Qu and Leahy, 1995), respectively. This is a clear indication that the widely open conical groove affords a very loose home to the α7 helix, which can line along the entrenchment (in the metal-free α_L I domain and α_M I domain) or much tilted (in HA or metal-chelating α_L I domain) or even in an upside-down orientation (in the dm-I domain of the ICAM-5 complex).

It is particularly interesting to further examine the three α7 helices embedded in the entrenchment. Figure 3B is a local side view of the groove with only these three helices. Successive hydrophobic side chains along the helix snugly extend into the entrenchment. From the top down, the closed form of metal-free α_L I domain (in blue) has Leu302, Ile306, and Tyr307, and the α_M I domain (in magenta) contains Ile308, Leu312, and Lys315. However, for the dm-I domain in the ICAM-5 complex (in yellow) there are Ile306, Leu302, and Leu298, in a reverse sequence. Since these side chains contribute to the major interactions, this explains why the α7 helix of dm-I domain from the ICAM-5 complex can fit in an upside-down fashion. We will discuss the biological significance of the positional diversity of α7 helix later.

The Interface and the Affinity

The ICAM-5 complex structure described here further confirms an identical binding mode of ICAM family members and reveals what affords dm-I domain "super-high" affinity to ICAM-5. The affinity of ICAM-5 binding to the dm-I domain was measured by surface plasmon resonance, and the Kd value was comparable to that of ICAM-3/HA, around 20 μM (Song et al., 2005). There are two conflicting factors affecting ICAM-5 binding affinity. The favorable one is fewer glycosylation sites on the binding domain D1 of ICAM-5 (2 glycans) than that on the D1 of ICAM-3 (5 glycans). This increases the on-rate of ICAM-5 binding compared to that of ICAM-3 (Song et al., 2005). The adverse factor is the less favored interface interactions. The surface buried area of ICAM-1/IA, ICAM-3/HA, and ICAM-5/dm-I domain is 2691 $Å^2$, 2347 $Å^2$, and 2259 $Å^2$, respectively, in agreement with the decreasing order of their integrin binding affinity. The binding interface of the ICAM family members is centered at the "hot spot," Glu37 for ICAM-2, ICAM-3, and ICAM-5 and Glu34 for ICAM-1. Figure S2

depicts the binding surfaces of three ICAMs. ICAM-5 appears similar to ICAM-3 in having fewer hydrophobic residues around the hot spot. A residue immediately adjacent to the hot spot is a hydrophobic residue, which strongly contributes to the binding energy. It is Leu66 in ICAM-3 and Met64 in ICAM-1 (Figure S2). Three hydrophobic residues, Leu204, Leu205, and Met140, of the I domain wrap around this hydrophobic residue from ICAMs, making intimate interactions. Intriguingly, ICAM-5 has Val67 with a shorter side chain in place (Figure S2). The ''missing'' methylene group of Val67 will leave a less favorable fit between the two binding partners in the ICAM-5/I domain interface. Since this less favorable fit, albeit at a small scale, is near the center of binding interface, it will significantly decrease the affinity.

The ICAM-5 complex structure also reveals structural features of the double mutation F265S/F292G that give rise to super-high affinity to the I domain. The Phe292 sits right at the tip of the critical β6α7 loop. In the closed form of the α_L I domain, this Phe292 residue extends its phenyl ring into a relatively hydrophobic pocket (Figure 3B). When the I domain undergoes conformational changes upon ligand binding, the β6α7 loop actually changes most of all so that the α7 helix can move axially as much as 7 Å (Shimaoka et al., 2002). During this process, energy penalty has to pay to shift the phenyl side chain of Phe292 out of the pocket and expose it to solvent (Figure 2A). A F292G mutant apparently no longer suffers from this problem. The unusual swing-out behavior of the α7 helix may reflect the ability of Gly to assume a wider range of the backbone conformational angles as predicted based on the F292A mutation (Jin et al., 2006). The effect of the F265S mutation is more exquisite. As shown in the Figure 2C, upon ligation, the movement of MIDAS residue Asp239 will drag the β4α5 loop with it (shown in yellow arrow). The moved loop in turn squeezes the otherwise totally buried phenyl ring of Phe265 out (compare the magenta ring in closed form to the cyan ring in ligated form in Figure 2C), becoming partially exposed. To have a smaller hydrophilic Ser in place of bulky hydrophobic Phe gains so much advantage. It not only makes a conformational transition easier but also offers a hydroxyl side-chain group to form a bidentate hydrogen bond (along with its main-chain amide group) to the carbonyl oxygen of Gly262, further stabilizing the open conformation (Figure 2C).

DISCUSSION

We have previously noticed a high mobility of the α7 helix and discussed a ratchet-like movement of the β6α7 loop in a hydrophobic pocket, resulting in the corresponding axial displacement of the α7 helix by one or two helical turns in the intermediate and open conformations of the α I domain, respectively (Shimaoka et al., 2003). The hydrophobic pocket that acts as a detent for the movement of the β6α7 loop is located above the conical groove that holds the α7 helix (Figure 3B). The results we have obtained from the ICAM-5/dm-I domain complex structure, combined with other structures, further demonstrate the intrinsic character of the conical groove that allows for the unusually free mobility of the α7 helix. The α7 helix can be forced to tilt away from the deep entrenchment by an engineered disulfide (HA in the ICAM-3 complex, green in Figure 3A). It can fit in the entrenchment within the groove (metal-free form, blue in Figure 3A) and swing out from the groove (Mn-bound form, cyan in Figure 3A). It can even take an upside-down orientation (dm-I domain in this work, yellow in Figure 3A). We appreciate that some of these observations can result from crystal packing artifacts or the protein engineering and are not necessarily physiological. Nevertheless, the important point here is that the demonstrated ''loose'' groove allows the α7 helix to move around and transmit the allosteric signal between domains with little energy penalty. Cell adhesion in general involves multivalent interactions in a dynamic process with each individual pair of interaction being very weak (Wang, 2002). An ''easy'' key signaling event manifest in the α7 helix movement in ICAM/integrin interaction described here provides an example of how this kind of weak adhesion interaction works in signaling.

The ICAM-5 complex structure confirms the role of ICAM-5 as an adhesion molecule in integrin-mediated cell-cell interactions in the central nervous system (Tian et al., 1997). Like other endothelial ICAM family members, only the N-terminal domain of neuronal ICAM-5 is involved in a stereotypical engagement with integrin's I domains. We have previously proposed possible molecular mechanisms, by which the two-domain ICAM-2 and the five-domain ICAM-1 present their key ligand-binding residue Glu on cell surface for integrin interaction. In the case of ICAM-2, a tripod-like glycan distribution on the membrane-proximal domain 2 helps orient Glu37 (Casasnovas et al., 1997). In the case of ICAM-1, the intimate dimerization of domain 4 and the stem-like stiff linkage between domains 4 and 5 near cell membrane present Glu34 at N-terminal domain for interaction (Yang et al., 2004). ICAM-5 is composed of nine Ig-like domains. The sequence similarity between ICAM-1 and the D1-D5 of ICAM-5 seems to imply that ICAM-5 might have a similar architecture for its first five Ig domains. It will be interesting in the future to visualize how this long nine-domain molecule is organized on cell surface to perform both homophilic and heterophilic interactions.

EXPERIMENTAL PROCEDURES

Preparation of the N-Terminal Two-Domain Fragment of ICAM-5

The N-terminal two-domain fragment of ICAM-5 was expressed in the lectin-resistant CHO-Lec 3.2.8.1 cells. A recombinant cDNA coding for residues 1 to 227 of the precursor protein (Mizuno et al., 1997) followed by a translation stop codon was generated by PCR and cloned into the unique XhoI site of the pBJ5-GS expression vector. CHO-Lec cells were transfected with the recombinant vector, and clones secreting the soluble ICAM-5 protein were selected as described elsewhere (Casasnovas et al., 1997, 1998). The protein was purified by multistep chromatography using ion-exchange columns SP-sepharose (Amersham Biosciences), Mono Q, and Mono S and a size-exclusion Superdex-75 column. The purified protein was concentrated up to 40 mg/ml for crystallization trials in 20 mM HEPES (pH 7.5) and 50 mM sodium chloride.

Expression of Soluble I Domain and Surface Plasmon Resonance Measurement

The αL dm-I domain was expressed in *E. coli*, refolded, and purified as described (Shimaoka et al., 2003). The purified protein was dissolved in 20 mM Tris-HCl (pH 8.0) and 50 mM NaCl. ICAM-5-coupled or BSA-coupled CM5 sensor chip as control was prepared with the amine coupling kit (Biacore) as described (Shimaoka et al., 2001). Surface plasmon resonance was measured by using a Biacore 3000 optical biosensor. I domain was injected over the chip in 20 mM Tris HCl (pH 8.0), 150 mM NaCl, and 10 mM $MgCl_2$, at a flow rate of 10 μl/min at 25°C.

Crystallization and Structure Determination

ICAM-5 was mixed with equal molar of dm-I domain to a total protein concentration of 15 mg/ml. Crystals were obtained by the hanging droplet vapor diffusion method with the reservoir buffer in 0.1 M HEPES (pH 7.5), 7.5% PEG 8000, 10% glycerol, and 5 mM $MgCl_2$. They were harvested and soaked in 0.1 M HEPES (pH 7.5), 15% PEG 8000, 20% glycerol, and 5 mM $MgCl_2$ before freezing. The diffraction data were collected at 19ID at Argonne National Laboratory and processed with HKL2000 (Otwinowski and Minor, 1997). Molecular replacement was used to determine the structure. ICAM-3/HA (PDB code 1T0P) and the second domain of ICAM-1 (PDB code 1IC1) were used as search models. The structure was refined with CNS and Refmac (CCP4, 1994) to R = 19.08% and R_{free} = 23.49%. The model was validated with MolProbity (Davis et al., 2007).

ACCESSION NUMBERS

The coordinates of the complex structure have been deposited in the PDB with the code 3BN3.

SUPPLEMENTAL DATA

The Supplemental Data include two figures and can be found with this article online at http://www.molecule.org/cgi/content/full/31/3/432/DC1/.

ACKNOWLEDGMENTS

We thank staff members at Advanced Photon Source for beam time help. This work was supported by grants from the NIH to J.-h.W. and T.A.S., the Academy of Finland and the Sigrid Jusélius Foundation to C.G.G., and the MEC of Spain (BFU2005-05972) to J.M.C.

Received: December 21, 2007
Revised: April 9, 2008
Accepted: June 27, 2008
Published: August 7, 2008

REFERENCES

Casasnovas, J.M., Springer, T.A., Liu, J.H., Harrison, S.C., and Wang, J.-H. (1997). Crystal structure of ICAM-2 reveals a distinctive integrin recognition surface. Nature *387*, 312–315.

Casasnovas, J.M., Stehle, T., Liu, J.-H., Wang, J.-H., and Springer, T.A. (1998). A dimeric crystal structure for the N-terminal two domains of intercellular adhesion molecule-1. Proc. Natl. Acad. Sci. USA *95*, 4134–4139.

CCP4 (1994). The CCP4 suite: programs for protein crystallography. Acta Crystallogr. *D50*, 760–763.

Davis, I.W., Leaver-Fay, A., Chen, V.B., Block, J.N., Kapral, G.J., Wang, X., Murray, L.W., Arendall, W.B., III, Snoeyink, J., Richardson, J.S., and Richardson, D.C. (2007). MolProbity: all-atom contacts and structure validation for proteins and nucleic acids. Nucleic Acids Res. *35*, W375–W383.

Emsley, J., Knight, C.G., Farndale, R.W., Barnes, M.J., and Liddington, R.C. (2000). Structural basis of collagen recognition by integrin alpha2beta1. Cell *101*, 47–56.

Gahmberg, C.G. (1997). Leukocyte adhesion: CD11/CD18 integrins and intercellular adhesion molecules. Curr. Opin. Cell Biol. *9*, 643–650.

Hynes, R.O. (2002). Integrins: bidirectional, allosteric signaling machines. Cell *110*, 673–687.

Jin, M., Song, G., Carman, C.V., Kim, Y.S., Astrof, N.S., Shimaoka, M., Wittrup, D.K., and Springer, T.A. (2006). Directed evolution to probe protein allostery and integrin I domains of 200,000-fold higher affinity. Proc. Natl. Acad. Sci. USA *103*, 5758–5763.

Lee, J.O., Rieu, P., Arnaout, M.A., and Liddington, R. (1995). Crystal structure of the A domain from the alpha subunit of integrin CR3 (CD11b/CD18). Cell *80*, 631–638.

Lindsberg, P.J., Launes, J., Tian, L., Valimaa, H., Subramanian, V., Siren, J., Hokkanen, L., Hyypia, T., Carpen, O., and Gahmberg, C.G. (2002). Release of soluble ICAM-5, a neuronal adhesion molecule, in acute encephalitis. Neurology *58*, 446–451.

Luo, B.H., Carman, C.V., and Springer, T.A. (2007). Structural basis of integrin regulation and signaling. Annu. Rev. Immunol. *25*, 619–647.

Mizuno, T., Yoshihara, Y., Inazawa, J., Kagamiyama, H., and Mori, K. (1997). cDNA cloning and chromosomal localization of the human telencephalin and its distinctive interaction with lymphocyte function-associated antigen-1. J. Biol. Chem. *272*, 1156–1163.

Mizuno, T., Yoshihara, Y., Kagamiyama, H., Ohsawa, K., Imai, Y., Kohsaka, S., and Mori, K. (1999). Neuronal adhesion molecule telencephalin induces rapid cell spreading of microglia. Brain Res. *849*, 58–66.

Mori, K., Fujita, S.C., Watanabe, Y., Obata, K., and Hayaishi, O. (1987). Telencephalon-specific antigen identified by monoclonal antibody. Proc. Natl. Acad. Sci. USA *84*, 3921–3925.

Oka, S., Mori, K., and Watanabe, Y. (1990). Mammalian telencephalic neurons express a segment-specific membrane glycoprotein, telencephalin. Neuroscience *35*, 93–103.

Otwinowski, Z., and Minor, W. (1997). Processing of X-ray diffraction data collected in oscillation mode. In Macromolecular Crystallography, C.W. Carte, Jr. and R.M. Sweet, eds. (San Diego, London, Boston, New York, Sydney, Tokyo, Toronto: Academic Press), pp. 307–326.

Qu, A., and Leahy, D.J. (1995). Crystal structure of the I-domain from the CD11a/CD18 (LFA-1, alpha L beta 2) integrin. Proc. Natl. Acad. Sci. USA *92*, 10277–10281.

Shimaoka, M., Lu, C., Palframan, R., von Andrian, U.H., Takagi, J., and Springer, T.A. (2001). Reversibly locking a protein fold in an active conformation with a disulfide bond: integrin αL I domains with high affinity and antagonist activity in vivo. Proc. Natl. Acad. Sci. USA *98*, 6009–6014.

Shimaoka, M., Takagi, J., and Springer, T.A. (2002). Conformational regulation of integrin structure and function. Annu. Rev. Biophys. Biomol. Struct. *31*, 485–516.

Shimaoka, M., Xiao, T., Liu, J.H., Yang, Y., Dong, Y., Jun, C.D., McCormack, A., Zhang, R., Joachimiak, A., Takagi, J., et al. (2003). Structures of the alphaL I domain and its complex with ICAM-1 reveal a shape-shifting pathway for integrin regulation. Cell *112*, 99–111.

Song, G., Yang, Y., Liu, J.H., Casasnovas, J.M., Shimaoka, M., Springer, T.A., and Wang, J.H. (2005). An atomic resolution view of ICAM recognition in a complex between the binding domains of ICAM-3 and integrin alphaLbeta2. Proc. Natl. Acad. Sci. USA *102*, 3366–3371.

Springer, T.A., and Wang, J.H. (2004). The three-dimensional structure of integrins and their ligands, and conformational regulation of cell adhesion. Adv. Protein Chem. *68*, 29–63.

Tian, L., Yoshihara, Y., Mizuno, T., Mori, K., and Gahmberg, C.G. (1997). The neuronal glycoprotein telencephalin is a cellular ligand for the CD11a/CD18 leukocyte integrin. J. Immunol. *158*, 928–936.

Tian, L., Lappalainen, J., Autero, M., Hanninen, S., Rauvala, H., and Gahmberg, C.G. (2008). Shedded neuronal ICAM-5 suppresses T-cell activation. Blood *111*, 3615–3625.

Wang, J. (2002). Protein recognition by cell surface receptors: physiological receptors versus virus interactions. Trends Biochem. Sci. *27*, 122–126.

Yang, Y., Jun, C.-D., Liu, J.-H., Zhang, R., Joachimiak, A., Springer, T., and Wang, J.-H. (2004). Structural basis for dimerization of ICAM-1 on the cell surface. Mol. Cell *14*, 269–276.

Molecular Cell, Volume *31*

Supplemental Data

An Unusual Allosteric Mobility of the C-Terminal Helix of a High-Affinity α_L Integrin I Domain Variant Bound to ICAM-5

Hongmin Zhang, Jose M. Casasnovas, Moonsoo Jin, Jin-huan Liu, Carl G. Gahmberg, Timothy A. Springer, and Jia-huai Wang

Figure S1. Packing of ICAM-5/dm-I in the crystals

Symmetry related complexes are shown along a screw axis 2_1. α7 helix of the I domain swings out and fits into the groove of a symmetry related I domain.

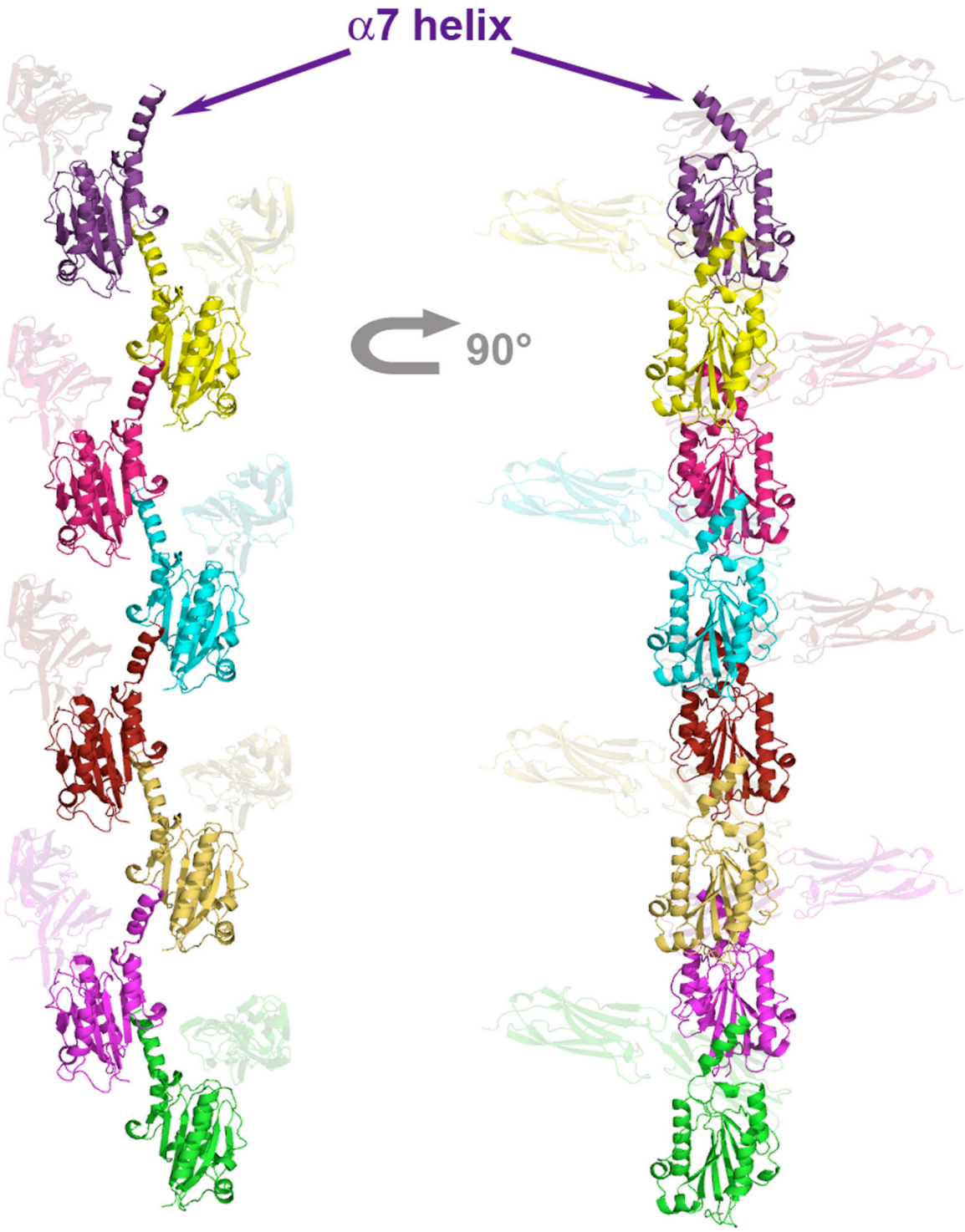
α7 helix
90°

Figure S2. Surface representations of the binding face of ICAM-1, ICAM-3 and ICAM-5

Negatively and positively charged residues are colored red and blue, respectively. Hydrophobic and neutral hydrophilic residues are colored grey and yellow, respectively. Some important residues are labeled. This figure is prepared with GRASP (Nicholls et al., 1991).

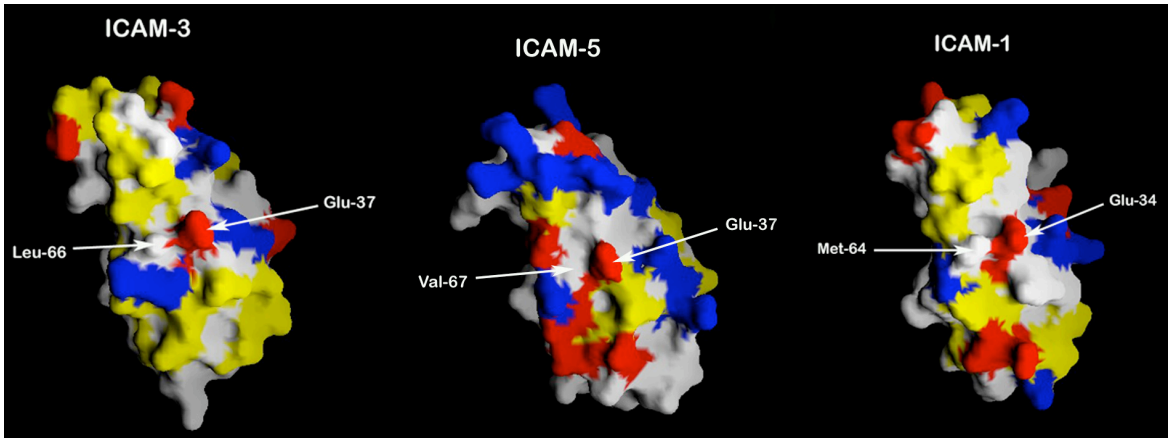

Supplemental Reference

Nicholls, A., Sharp, K.A., and Honig, B. (1991). Protein folding and association: insights from the interfacial and thermodynamic properties of hydrocarbons. Proteins *11*, 281–296.